applied microbiology

MDPI

Article

Enhanced Microbial Production of Caproic Acid via Chain Elongation Stimulated by Redox-Active Materials

Carolina Niño-Gómez [1], Denisse Serrano-Palacios [2], Edna R. Meza-Escalante [2], Refugio B. García-Reyes [3], Miguel A. Armenta [1], Lilian Torres-Montijo [1], Irina Cobos-Mercado [1], Vianey A. Burboa-Charis [1,*] and Luis H. Alvarez [1,*]

[1] Departamento de Biotecnología y Ciencias Alimentarias, Instituto Tecnológico de Sonora (ITSON), Ciudad Obregón 85000, Sonora, Mexico; docanigo@outlook.es (C.N.-G.); angel456_1@hotmail.com (M.A.A.); lilian.torres213296@potros.itson.edu.mx (L.T.-M.); irina.cobos204038@potros.itson.edu.mx (I.C.-M.)
[2] Departamento de Ciencias del Agua y Medio Ambiente, Instituto Tecnológico de Sonora (ITSON), Ciudad Obregón 85000, Sonora, Mexico; denisse.serrano@itson.edu.mx (D.S.-P.); edna.meza@itson.edu.mx (E.R.M.-E.)
[3] Facultad de Ciencias Químicas, Universidad Autónoma de Nuevo León (UANL), San Nicolás de los Garza 66455, Nuevo León, Mexico; refugio.garciary@uanl.edu.mx
* Correspondence: vburboach@gmail.com (V.A.B.-C.); luis.alvarez@itson.edu.mx (L.H.A.)

Abstract

This study examined whether the electron-transfer capacity (ETC) of redox-active materials affects caproic acid production in ruminal sediment cultures. Two carbon-based materials (granular activated carbon, GAC, and bituminous coal, BC), two iron oxides (magnetite and hematite), and two humic substances (Leonardite and Elliott) were characterized for ETC with glucose or ethanol/acetic acid (EtOH/HAc) and then tested in batch cultures. All materials exhibited ETC, with higher values for glucose (0.2–1.1 mEq/g) than for EtOH/HAc (0.09–0.2 mEq/g). BC and GAC yielded the highest caproic acid concentrations (31.6 and 29.3 mM, respectively; 67% and 55% above the control). FTIR revealed quinone-type C=O groups in both materials and in Elliott. Magnetite, hematite, and Elliott reached approximately 26 mM (37% above the control). Leonardite, which was dominated by carboxyl groups, reduced production by 70.3%. ETC did not predict caproic acid production across all materials because surface chemistries differed; however, it showed a positive correlation specifically among quinone-bearing materials and hematite. In a second assay, co-feeding glucose with EtOH/HAc reduced caproic acid production by 21.6–44.4% compared with cultures fed EtOH/HAc alone, suggesting that glucose prompted a distinct fermentation pathway. Thus, carbon-based materials, particularly BC, enhanced chain elongation most effectively, whereas glucose provided no additional benefit.

Keywords: chain elongation; anaerobic microorganisms; electron transfer; biorefineries

Check for updates

Academic Editor: Ermenegilda Parrilli

Received: 23 October 2026
Revised: 22 November 2026
Accepted: 23 November 2026
Published: 25 November 2026

Copyright: © 2026 by the authors. Licensee MDPI, Basel, Switzerland. This article is an open access article distributed under the terms and conditions of the Creative Commons Attribution (CC BY) license.

1. Introduction

Biorefineries convert raw materials into specialty chemicals and alternative energy [1,2]. Anaerobic biorefineries, initially limited to hydrogen and methane, now also yield high-value intermediates, including short- and medium-chain fatty acids (MCFA) [3]. Among these, caproic acid is a versatile precursor of flavoring compounds, aviation fuels [4], natural antimicrobials [5], and cosmetics [6]. Producing MCFA by microbial chain elongation is more environmentally friendly and sustainable [7], and the strong market potential of caproic acid enhances the economic viability of bioconversion [8].

Chain elongation relies on the reverse β-oxidation pathway in anaerobic digestion, which converts electron donors (e.g., ethanol) and acetate into higher-value carboxylates such as caproic acid [9]. This pathway conserves energy and directs carbon toward energy-dense products [10]. However, electron-transfer kinetics, the chemiosmotic gradient [11], and limited electron-donor availability [12] reduce yields and limit industrial scale-up.

One strategy to overcome these limitations is to add redox-active materials, which may facilitate electron flow within microbial communities and enhance chain elongation [13]. Carbon-based materials, iron oxides, humic substances, and model quinones are promising options for MCFA production [13,14]. They act through redox-active functional groups such as quinones, which provide electron-transfer capacity (ETC) [15], or, in carbon-based materials, through electron conduction across their structure [16]. By contrast, iron oxides accept electrons by reducing Fe(III) to Fe(II) [17]. Humic substances owe much of their redox activity to quinone groups [18]. To our knowledge, carbon-based materials have been widely studied for chain elongation, while the effects of iron oxides and humic substances remain largely unexplored. For instance, biochar from digested sludge with the highest electron-transfer efficiencies increased caproic acid production and enriched *Clostridium kluyveri*, *Clostridium magnum*, and *Clostridium botulinum*, which are associated with chain elongation; the biochar exhibited strong redox activity due to surface quinones and hydroquinones [19].

The ETC requires a material to first accept electrons (reduction) and then donate them (oxidation) under conditions that favor microbial processes. Under anaerobic or microaerobic conditions, many bacteria use extracellular electron transfer to pass electrons to distant acceptors (e.g., carbon-based materials or iron oxides), independently of classical respiratory chains [20]. *C. kluyveri*, a typical chain-elongating bacterium, does not interact with electrodes, suggesting that it lacks this mechanism. Instead, its high caproic acid production with biochar was associated with material properties such as bacterial attachment and adsorption of inhibitory compounds; in contrast, other *Clostridium* species, such as *C. pasteurianum*, *C. ljungdahlii*, and *C. aceticum*, can participate in bioelectrosynthesis [21]. This suggests that mixed cultures are better suited for chain elongation in the presence of redox-active materials.

Whether the ETC of a material predicts its effect on chain elongation remains unclear. Microbial ETC is typically measured using glucose, which microorganisms oxidize while reducing the electron acceptor; in contrast, chain elongation here relies on EtOH/HAc. Previous work showed that adding glucose inhibited caproic acid synthesis in *Lacrimispora celerecrescens* cultures because glucose was preferentially consumed over ethanol, yielding mainly lactic acid [22]. Glucose could nevertheless supply electrons to reduce redox-active materials, thereby offsetting this diversion and promoting MCFA production. This study evaluated six materials (two carbon-based, two iron oxides, and two humic substances) by measuring their ETC and testing their effects on caproic acid production with EtOH/HAc, both alone and with added glucose.

2. Materials and Methods

2.1. Inoculum Preparation and Basal Medium

Bovine ruminal sediment from a slaughterhouse in Ciudad Obregón, México, served as the inoculum. The sediment was oven-dried at 50 °C for 24 h, then crushed and sieved to obtain particles <425 µm. The sediment was then hermetically stored at 4 °C and used directly without acclimatization. The basal medium contained (g/L): 0.31 K_2HPO_4, 0.23 KH_2PO_4, 0.25 NH_4Cl, 0.20 $MgSO_4 \cdot 7H_2O$, 1.5 $NaHCO_3$, and 22.2 mL ethanol (to 380 mM) and 5.3 mL acetic acid (to 92 mM). To inhibit methanogenesis, a stock solution of 2-bromoethanesulfonic acid (BES) was added to achieve a final concentration of 50 mM. To promote fermentative

conditions and limit methanogenesis, the pH was adjusted to 6.5 with HCl. N_2 gas was bubbled through the liquid medium to establish anaerobic conditions.

2.2. Selection and Characterization of Redox Materials

Six materials were evaluated as additives to fermentative cultures to assess their potential to increase caproic acid production. Granular activated carbon (GAC) (Clarimex, Monterrey, NL, México) and bituminous coal (BC) (Carbotecnia, Zapopan, JAL, México) were selected as the carbon-based materials. These materials were crushed and sieved to obtain particles between 425 and 600 μm, then washed with distilled water to remove fine powder and dried at 50 °C for 24 h. The iron oxides were magnetite (Fe_3O_4, stock #2650TS) and hematite (Fe_2O_3, stock #2520ZH), with particle sizes of 50–100 nm and 30–50 nm, respectively (Nanostructured & Amorphous Materials Inc., Katy, TX, USA). The selected humic substances were Leonardite (1BS104L) and Elliott (1BS102M), used as received from the supplier (International Humic Substances Society, St. Paul, MN, USA).

The electron-transfer capacity (ETC) of the six materials was evaluated using the ferrozine assay described by Lovley et al. [23]. Briefly, experiments were conducted in 60 mL serological bottles containing 10 mL of basal medium, which were thoroughly purged with N_2 to ensure strictly anaerobic conditions. For each material (1 g/L), triplicate bottles were inoculated with the dried sediment at 1 g volatile suspended solids (VSS)/L. Aliquots of stock solutions of EtOH/HAc (ethanol/acetic acid) and glucose were added to achieve final concentrations of 42.5 g COD/L (5312 mEq/L) and 2.15 g COD/L (269 mEq/L), respectively. These values correspond to the EtOH/HAc concentration in the basal medium and the typical glucose concentration used in the ETC assay. Notably, the electron equivalents are very low in the glucose-containing medium.

Control assays without added materials were also prepared in triplicate for each substrate under identical experimental conditions. All bottles were incubated at 150 rpm and 37 °C for 48 h. Fe(III) citrate was then added to a final concentration of 10 mM, and the mixture was allowed to react for 15 min. An equal volume of 0.5 M HCl was added to each sample, and a 0.2 mL aliquot was mixed with 4.8 mL of ferrozine solution to determine Fe(II) spectrophotometrically at 562 nm. The Fe(II) concentration was used to calculate the ETC from all materials to Fe(III). All ETC measurements were corrected ($Fe(II)_{net} = Fe(II)_{sample} - Fe(II)_{control}$) for the intrinsic capacity of anaerobic sludge to reduce Fe(III), minimizing interference from redox-active molecules in the sludge. ETC was normalized by material mass: ETC ($mEq/g_{material}$) = $Fe(II)_{net}$ (mEq/L)/Concentration of material ($g_{material}$/L).

The surface functional groups of GAC, BC, magnetite, hematite, Leonardite, and Elliott were characterized using Fourier transform infrared spectroscopy (FTIR) with a Nicolet 6700 spectrometer (Thermo Fisher Scientific, Madison, WI, USA) at a resolution of 4 cm^{-1}.

2.3. Batch Fermentation Experiments

Fermentative cultures for caproic acid production were prepared in triplicate in 120 mL serological bottles with an 80 mL working volume. Each bottle was inoculated with dried sediment at 5 g VSS/L. Depending on the treatment, cultures were supplemented with carbon-based materials (5 g/L), iron oxides (250 mg/L), or humic substances (250 mg/L). After sealing the bottles with butyl rubber stoppers, the headspace was thoroughly flushed with N_2 gas to remove residual oxygen and establish strict anaerobic conditions. Cultures were then incubated at 37 °C on a rotary shaker at 150 rpm for 24 days. Cumulative volume of biogas was quantified by the liquid displacement method, using a 2% (*w*/*v*) NaOH solution to trap and sequester CO_2.

A second set of independent triplicate experiments was conducted under identical basal medium (including EtOH/HAc) and environmental conditions, with only the top-

performing material from each category selected in the first assay. Glucose pulses from a stock solution were added every five days (on days 0, 5, 10, 15, and 20), bringing the concentration to 2 g/L with each addition. Controls without material, both with and without glucose, were included. The experiment tested whether an additional electron source could enhance the reduction in redox-mediating groups in the materials.

Kinetic parameters for caproic acid production were derived from the experimental data using the following modified Gompertz model (Equation (1)):

$$P(t) = P_{max} \times \exp\left[-\exp\left[\frac{2.71828 \times R_{max}}{P_{max}}(\lambda - t) + 1\right]\right] \quad (1)$$

where P is the cumulative caproic acid production (mM), P_{max} is the maximum production (mM), R_{max} is the production rate (mM/day), t is time (days), and λ is the lag phase (days). The parameters were estimated in Statistica 11.0 by minimizing the sum of squared residuals between the experimental data and the model curves.

2.4. Adsorption of Substrates and Products on Materials

To assess the potential adsorption of substrates (ethanol and acetic acid) and soluble metabolic products (short- and medium-chain volatile fatty acids) onto the materials, independent abiotic adsorption experiments were conducted for each material. This assay determined whether the target compounds exhibited restricted bioavailability or whether their final concentrations were underestimated due to physical entrapment at the end of the incubation period.

Serological bottles (120 mL) containing 80 mL of inoculum-free basal medium were prepared in triplicate and supplemented with carbon-based materials (5 g/L), iron oxides (250 mg/L), or humic substances (250 mg/L). Each bottle was spiked with an aliquot of a stock solution containing ethanol, acetic acid, propionic acid, butyric acid, valeric acid, and caproic acid to achieve a final equimolar concentration of 20 mM for each compound. The bottles were hermetically sealed with rubber stoppers and aluminum crimps, then incubated on a rotary shaker at 37 °C and 150 rpm for 7 days. Initial and final concentrations were quantified by gas chromatography to calculate the net adsorption efficiency (%).

2.5. Analytical Methods

VSS concentrations were determined according to Standard Methods. Ethanol and short- and medium-chain VFAs were quantified using a gas chromatograph (Nexis GC-2030, Shimadzu Scientific Instruments, Inc., Columbia, MD, USA equipped with an autoinjector (AOC-30 series, Shimadzu) and a flame ionization detector (FID). Chromatographic separation was performed on a Stabilwax capillary column (30 m × 0.32 mm i.d. × 1 µm film thickness). Prior to analysis, liquid samples were centrifuged at 7000 rpm for 5 min, acidified with 10% (*v*/*v*) phosphoric acid, and filtered through 0.22 µm membrane filters to remove particulate matter and ensure chromatographic stability. N_2 served as the carrier gas at a constant flow rate of 2.0 mL/min. Liquid samples (10 µL) were injected in split mode. The injector and detector temperatures were maintained at 200 °C. The oven temperature program started at 70 °C (held for 1 min), ramped to 230 °C at 10 °C/min, and was held at 230 °C for 1 min.

Hydrogen and methane (%) in the headspace were measured by gas chromatography equipped with a thermal conductivity detector (TCD) and a stainless-steel packed column. A 100-µL gas sample was collected from the headspace using a gas-tight syringe (Hamilton Co., Reno, NV, USA) and manually injected. N_2 was used as the carrier gas at a flow rate of 25 mL/min. The injector, oven, and detector temperatures were maintained at 250 °C, 70 °C, and 250 °C, respectively.

2.6. Statistical Analysis

All experiments were performed in triplicate with independent bottles. Data are reported as mean ± standard deviation, except for the Gompertz parameters (P_{max}, R_{max}, and λ), which are shown as box-and-whisker plots. Gompertz parameters were estimated separately for each replicate bottle. Mean ETC, caproic acid concentrations, cumulative hydrogen, and Gompertz parameter values were tested for statistically significant differences using analysis of variance (ANOVA), followed by Tukey's post hoc test for single-factor ANOVA ($\alpha = 0.05$). Pearson correlations between ETC and caproic acid production were calculated using treatment means. All statistical analyses were performed in Minitab 20.

3. Results and Discussion

3.1. Influence of Substrates on ETC of Materials

All tested materials showed ETC when glucose or EtOH/HAc served as electron donors, as shown in Figure 1, but responses varied markedly with the conditions. Using glucose as an electron donor yielded higher ETC values (0.2 to 1.1 mEq/g) than EtOH/HAc (0.09 to 0.2 mEq/g). In all cases except the cultures with Leonardite, the means differed significantly between the two substrates. The capacity of the ruminal sediment to use the materials as electron acceptors varied between the two substrates, with the highest ETC values observed for glucose, despite its initial concentration (mEq/L) being ~20 times lower than that of EtOH/HAc. Microbial glucose oxidation uses the six materials as electron acceptors. Conversely, for EtOH/HAc oxidation, competition for electrons between material reduction and chain elongation in caproic acid production presumably explains the low ETC observed. Section 3.3 discusses this phenomenon.

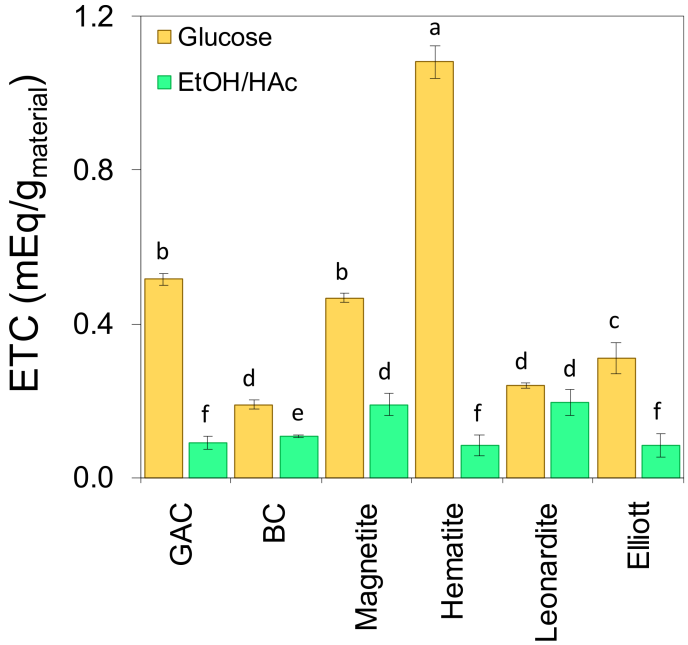


Figure 1. Electron-transfer capacity (ETC) of the six redox-active materials using glucose or ethanol/acetic acid (EtOH/HAc) as an electron donor. Bars show mean ± standard deviation. Different letters indicate significant differences among all treatments and substrate conditions ($p < 0.05$).

The ability of carbon-based materials and humic substances to accept electrons during glucose oxidation is linked to redox-active functional groups in their structures. Oxygenated groups such as quinones (C=O) primarily drive the reduction in these two materials [15,24]. In addition, non-oxygenated groups such as nitrogenous and sulfurous groups, which are

typically present in humic substances, have also been identified as contributing to the ETC [18]. For iron oxides, electron acceptance occurs via the reduction of Fe(III) to Fe(II), thereby solubilizing the iron [25].

3.2. Performance of Chain Elongation Using Redox-Active Materials

3.2.1. Caproic Acid Production and Consumption of Substrates

All cultures produced caproic acid, with profiles varying by material, as shown in Figure 2A. This response showed the capacity of ruminal sediment to promote caproic acid chain elongation. In almost all conditions, the inoculum adaptation period for caproic acid production was 7 days, consistent with times reported in other studies [26,27]. The two carbon-based materials yielded the highest caproic acid production, achieving 31.6 mM with BC and 29.3 mM with GAC, corresponding to increases of 67% and 55%, respectively, relative to the control. Cultures with magnetite, hematite, and Elliott produced a similar caproic acid concentration (~26 mM), 37% higher than the control. In contrast, Leonardite delayed caproic acid production until day 13 and showed the lowest production at the end of incubation, 70.3% lower than the control.

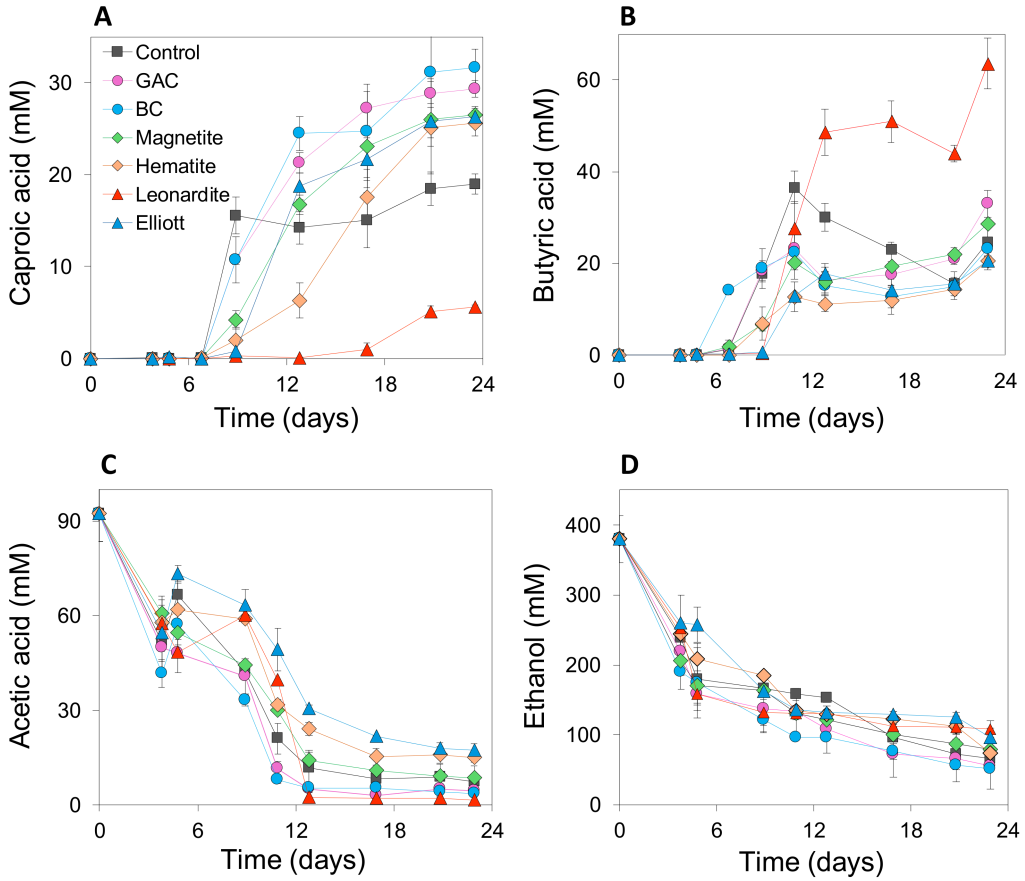


Figure 2. Performance of the chain elongation process in batch cultures of ruminal sediment amended with redox-active materials and in the control with EtOH/HAc as substrate. Time courses of (**A**) caproic acid production, (**B**) butyric acid production, (**C**) acetic acid consumption, and (**D**) ethanol consumption over 24 days of incubation. Data points show mean ± standard deviation.

Figure 2C,D show the acetic acid and ethanol concentration profiles over time, respectively. During the first 4 days, acetic acid was consumed; then its concentration increased slightly over 1–2 days, likely due to ethanol-oxidizing acetogenic bacteria, as previously observed by Ma et al. [28]. After this brief period of acetic acid production, its concentration declined alongside caproic acid production. By day 13, consumption reached 94% in the

BC and GAC cultures. Cultures containing the other materials achieved 81–90% removal by the end of the incubation period. Total ethanol consumption in GAC (85%) and BC (86%) cultures was higher than in the other conditions, relative to the initial ethanol concentration. Leonardite achieved the lowest ethanol consumption (71%). Ethanol and acetic acid consumption align with the behavior observed during caproic acid production.

Abiotic experiments showed that the two carbon-based materials and the two iron oxides adsorbed substrates such as ethanol and acetic acid, as well as liquid products including caproic, butyric, valeric, and propionic acids (Figure 3). This adsorption may influence the fermentation process. BC exhibited the highest adsorption rates among the six compounds tested, ranging from 6% to 23%, with the highest values for acetic and caproic acids. GAC adsorbed all five organic acids at levels ranging from 4% to 9.6% but did not adsorb ethanol. Hematite and magnetite adsorbed between 1% and 6%, although magnetite did not adsorb caproic acid or ethanol. The primary mechanism for organic acid adsorption onto activated carbon is electrostatic attraction between the negatively charged carboxylate groups (R-COO-) of the acids and the positively charged sites on the activated carbon. Additionally, hydrophobic interactions between the aliphatic chains of organic acids and the activated carbon surface have been reported [29].

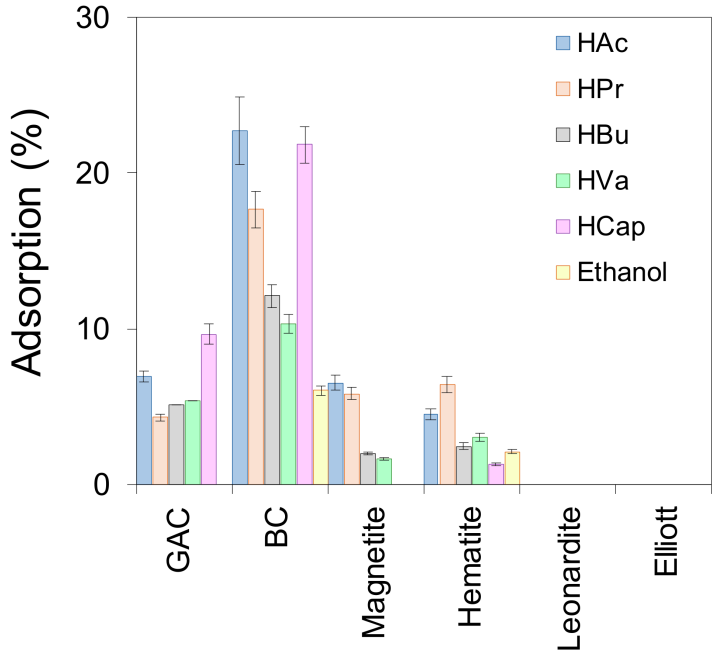


Figure 3. Adsorption of substrates and liquid products onto the redox-active materials under abiotic conditions. Bars show mean ± standard deviation.

The final concentrations of substrates and products measured in the cultures may be underestimated due to adsorption, particularly onto carbon-based materials and iron oxides. This physical removal of compounds from the liquid phase directly lowers their detectable concentrations and simultaneously reduces substrate bioavailability for the microorganisms. Consequently, this limited availability can reduce overall system productivity by slowing the fermentation process [30]. Because caproic acid was specifically adsorbed to GAC, BC, and hematite, its actual final concentration could be considerably higher, given that a significant fraction of it, most notably in the case of BC, remains bound to the material (Table 1).

Table 1. Estimated caproic acid production in microbial cultures assisted by redox materials, corrected for material adsorption.

	Liquid-Phase Concentration [a] (mM)	Adsorbed Fraction [b] (%)	Estimated Concentration [c] (mM)
GAC	29.3	9.6	32.4
BC	31.6	21.8	40.4
Magnetite	26.5	0.0	26.5
Hematite	25.6	1.3	25.9
Leonardite	5.6	0.0	5.6
Elliott	26.3	0.0	26.3

[a] Caproic acid concentration in the liquid phase at the end of the incubation period (Figure 2A). [b] Fraction of caproic acid adsorbed in each material under abiotic conditions (Figure 3). [c] Estimated concentration = concentration in the liquid phase/(1 − (adsorbed fraction/100)).

3.2.2. Other Fermentative Products

Butyric acid production occurred in all cultures, each with a distinct profile (Figure 2B). The lag phase occurred between days 5 and 9, depending on the material used. From day 11 to 21, net butyric acid production did not change markedly in the material-containing cultures, but it decreased in the control culture; the concentration then increased considerably in the last three days. Low caproic acid production in the Leonardite cultures was associated with high butyric acid production.

Propionic and valeric acids were also identified among the products, but their concentrations were relatively low across all cultures, ranging from 0.05 to 0.27 mM at the end of the incubation period (Figure S1). Organic acid production decreased the pH from an initial value of 6.5 to a final pH of 5.6–5.8 (Figure S2). Together, propionic and valeric acids represented a negligible fraction of the products compared with caproic acid, indicating that the process was selective toward even-chain carboxylates, with butyric acid as the main intermediate.

Hydrogen was a byproduct of chain elongation during caproic acid production (Figure 4). The lag phase for hydrogen was 7 days, matching that of caproic acid. Production continued until day 13, with GAC cultures achieving the highest values. In general, hydrogen production in the material-containing cultures was 1.17- to 1.52-fold higher than in the control. Hydrogen was the primary gaseous product identified (Figure S3); methane was not detected in any culture throughout the incubation period.

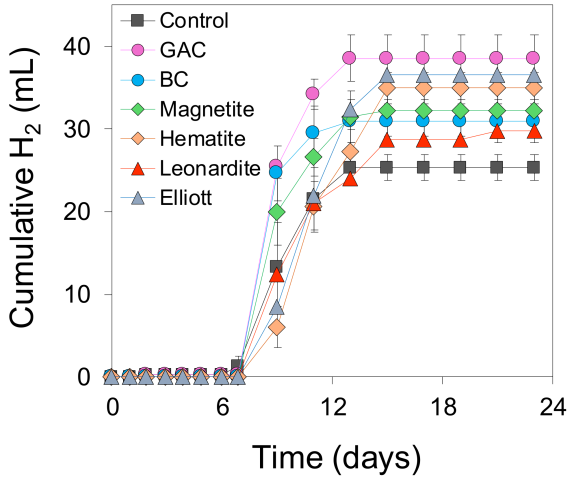


Figure 4. Hydrogen production profiles as a byproduct of chain elongation with the redox-mediating materials. Data points show mean ± standard deviation.

3.2.3. Kinetic Parameters for Caproic Acid Production

The modified Gompertz model was used to estimate kinetic parameters for caproic acid production from the collected experimental data. The resulting P_{max} values for the two carbon-based materials were significantly higher than those for all other evaluated materials, with the next highest values observed in the two iron oxides and Elliott (Figure 5A). Meanwhile, the highest R_{max} values were recorded in the BC and Elliott cultures at 2.4 mM/day, representing a rate 1.3-fold higher than that of the control group. Responses with GAC and hematite were 1.16- and 1.11-fold higher than the control, respectively. However, these differences among the four top materials were not statistically significant (Figure 5B). Finally, the lag phase showed the least variation across treatments, whereas the remaining cultures showed numerically longer lag phases (9–10 days); only Leonardite (~15 days) differed significantly (Figure 5C).

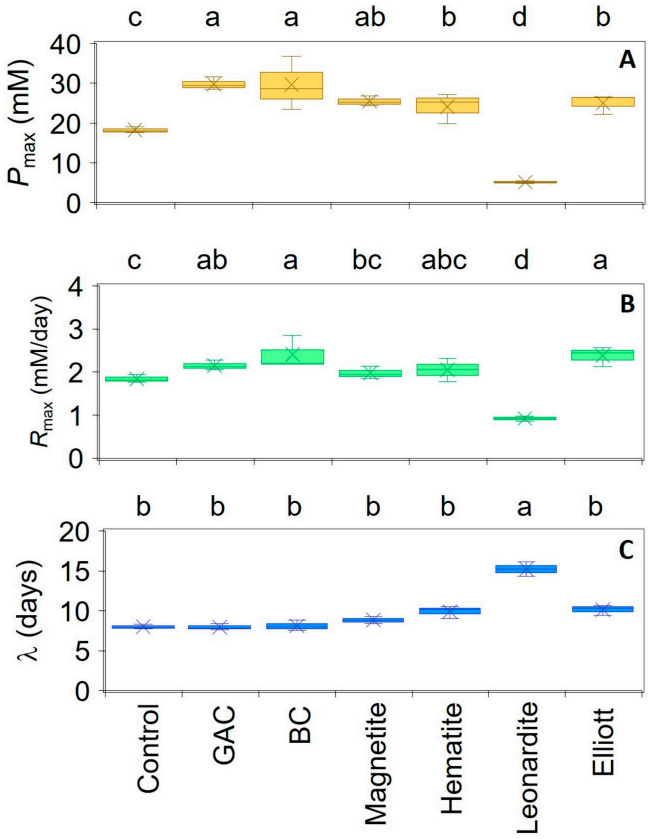


Figure 5. Kinetic parameters of caproic acid production estimated with the modified Gompertz model for cultures with redox-active materials and the control: (**A**) maximum caproic acid production (P_{max}), (**B**) maximum production rate (R_{max}), and (**C**) lag phase (λ, days). In each box, the horizontal line is the median, the cross (×) is the mean, and the lower and upper box limits are the first and third quartiles; whiskers extend to the minimum and maximum values, and no outliers were identified. Within each panel, different letters indicate significant differences among treatments ($p < 0.05$).

3.3. Impact of Glucose on Chain Elongation Using Redox-Active Materials

Glucose was added as an additional electron donor that could promote the reduction of redox-active materials, as suggested by the ETC assays (Figure 1). For this experiment, BC, hematite, and Elliott were selected, one material for each type, based on their performance in ETC determinations and caproic acid production. The materials substantially enhanced chain elongation, as indicated by caproic acid production, while glucose co-supplementation decreased caproic acid production in all cultures (Figure 6). In the absence of glucose,

the cultures with EtOH/HAc and BC showed the highest performance, achieving a maximum caproic acid concentration of ~70 mM. This represents a 94.4% increase relative to the control (36 mM). Supplementation with hematite (51 mM) and Elliott (45 mM) also increased production by 41.7% and 25% relative to the control, respectively, underscoring the functional role of redox-active materials in facilitating microbial metabolism.

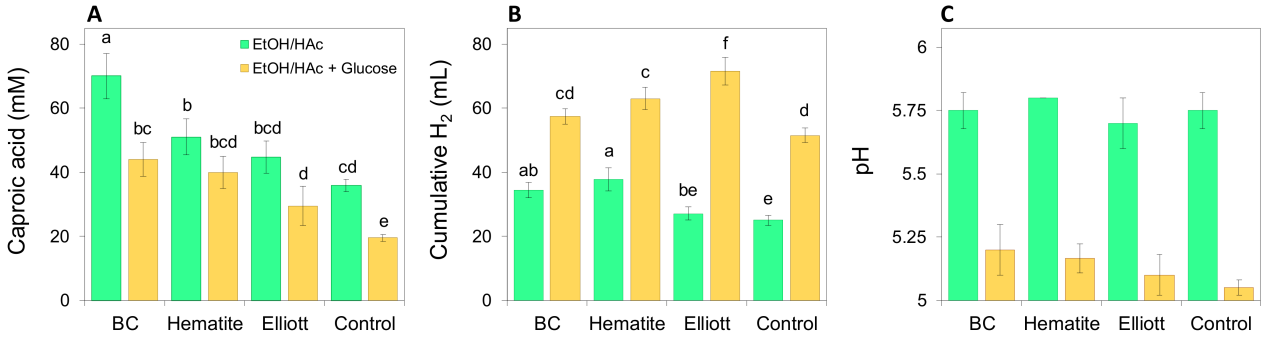


Figure 6. Effect of glucose co-feeding on chain elongation in ruminal cultures amended with BC, hematite, and Elliott, and in the control. (**A**) Maximum caproic acid concentration, (**B**) cumulative H_2 production, and (**C**) final pH. Bars show mean ± standard deviation. In panels (**A**,**B**), different letters indicate significant differences among all conditions ($p < 0.05$).

Microbial cultures supplemented with glucose (EtOH/HAc + glucose) altered product yields across all experimental groups. With glucose addition, caproic acid accumulation decreased by 37.1% in BC (~44 mM), 21.6% in hematite (~40 mM), 33.3% in Elliott (~30 mM), and 44.4% in the control (~20 mM), in comparison with their corresponding partner without glucose. The control with glucose, but without materials, yielded the lowest concentration among all tested conditions.

Cumulative hydrogen production showed the opposite response to glucose co-feeding (Figure 6B). With EtOH/HAc alone, hydrogen production was low in all cultures, although BC (34.5 mL) and hematite (37.8 mL) produced significantly more hydrogen than the control (25 mL), whereas Elliott (27.1 mL) did not differ from it. Glucose co-feeding increased cumulative hydrogen in all cultures by 67% in BC (57.5 mL), 67% in hematite (63 mL), 164% in Elliott (71.5 mL), and 106% in the control (51.4 mL), relative to their counterparts without glucose. In the presence of glucose, Elliott reached the highest hydrogen production among all conditions, and hematite also exceeded the control, whereas BC did not differ significantly from it. Therefore, the glucose-induced decrease in caproic acid coincided with increased hydrogen production, suggesting that glucose fermentation diverted electrons toward hydrogen evolution at the expense of reverse β-oxidation, consistent with a distinct fermentation pathway.

Although glucose could provide an additional electron source for reducing redox-active materials, it did not enhance caproic acid production; instead, it decreased it in all cultures (Figure 6A). Glucose may ferment faster than ethanol or acetate, favoring fast-growing acidogenic populations over chain-elongating bacteria. In cultures of *Lacrimispora celerecrescens* containing glucose and ethanol, glucose was preferentially consumed, supporting bacterial growth but limiting caproic acid production, while lactic acid accumulated and lowered the pH from 6.45 to 4.68 [22]. Our results show a similar trend: glucose addition lowered the pH from 6.5 to 5.05–5.2 (Figure 6C) and increased cumulative hydrogen production in all cultures (Figure 6B). Together, these observations suggest that glucose prompted a distinct fermentation pathway, with acidic products accumulating and reducing equivalents released as hydrogen rather than used for reverse β-oxidation. The lower pH may also have contributed to the decline in caproic acid, as undissociated carboxylic acids are toxic to

chain-elongating bacteria. The effect of glucose on chain elongation appears to depend on the microbial community and the culture conditions: adding glucose (4.12 g/L) promoted caproic acid production by *Clostridium butyricum* [31], whereas *Clostridium kluyveri* could not use it [32]. Overall, BC was the most effective additive for driving carboxylate chain elongation, while glucose co-feeding consistently suppressed caproic acid formation and enhanced hydrogen production.

3.4. Influence of Redox-Active Groups of Materials

Redox-active oxygenated functional groups, including quinone, carboxyl, and hydroxyl groups, in carbon-based materials and humic substances may promote electron transfer during chain elongation. All six materials showed ETC with either EtOH/HAc or glucose (Figure 1), likely due to their redox groups. Quinones are reported to be the primary electron-transfer groups in carbon-based materials [15] and humic substances [18]. They form a reversible redox pair (quinone + $2e^-$ + $2H^+$ ⇌ hydroquinone) and can cyclically accept and donate electrons [24]. Quinones also support chain elongation: modified biochar containing anthraquinone sulfonate (AQS) enhanced electron transfer and enriched microorganisms that support direct interspecies electron transfer (DIET), yielding 62% more caproic acid than the control without biochar, and C–O groups introduced by H_2O_2 oxidation also improved production [33].

The FTIR analysis links the surface chemistry of the materials to caproic acid production (Figure 7), focusing on quinone-type C=O groups, the main redox-active moieties of carbonaceous materials and humic substances [15,24]. In GAC and BC, the 1650–1550 cm^{-1} region (band at ~1575 cm^{-1}) combines aromatic C=C with conjugated quinone C=O (~1650–1510 cm^{-1}), and the band at ~1056 cm^{-1} corresponds to C–O/C–O–C of phenols, ethers, and lactones [34,35]. Quinone/hydroquinone couples within conductive aromatic domains can reversibly accept and donate electrons [24], and surface quinones enhance caproic acid synthesis [33]. Consistent with this, BC and GAC reached the highest caproic acid concentrations (31.6 and 29.3 mM; 67% and 55% above the control) and the highest ethanol consumption (86% and 85% of the initial ethanol).

Elliott shows quinone/aromatic bands (1650–1510 cm^{-1}), little carboxyl C=O (~1746 cm^{-1}), and silicate bands (~1021 and 798 cm^{-1}). It reached 26.3 mM caproic acid and the same maximum production rate as BC (R_{max} = 2.4 mM/day, 1.3-fold that of the control), consistent with quinones being the main electron acceptors in humic substances [18,36]. Leonardite has only a weak quinone C=O band (~1650 cm^{-1}) and is dominated by carboxyl groups: intense C=O at 1738 cm^{-1}, COO− at ~1558 and 1366 cm^{-1}, and C–O at 1216 cm^{-1}. This oxidized, carboxyl-rich matrix may divert electrons from reverse β-oxidation and hinder fermentative bacteria, as humic acid inhibited hydrolysis and *Clostridiales* [37]. Consistently, Leonardite delayed caproic acid production until day 13, gave the lowest final concentration (5.6 mM, 70.3% below the control), consumed the least ethanol (71%), and accumulated butyric acid.

Unlike humic substances, hematite and magnetite lack quinone functional groups. The bands of these Fe-based materials below ~700 cm^{-1} correspond to Fe–O vibrations (~540 and 560–580 cm^{-1}) [38]. Their moderate caproic acid production (25.6 and 26.5 mM, ~37% above the control) may therefore rely on Fe(III)/Fe(II) cycling rather than on quinones [3]. In this cycle, dissimilatory iron reduction uses microbial electrons to produce dissolved Fe(II) [39]. Dissolved Fe(II) can act as an extracellular electron shuttle, accelerating interspecies electron transfer [40]. Wang et al. [3] reported that Fe_2O_3 (20 g/L) promoted dissimilatory iron reduction and enzyme activity, and MCFA production was up to 2.4-fold higher than the control, mainly because crystalline Fe_2O_3 enhanced electron-transfer efficiency. In our study,

hematite increased caproic acid production 1.35-fold at 250 mg/L, 80 times lower than the concentration used by Wang et al. [3].

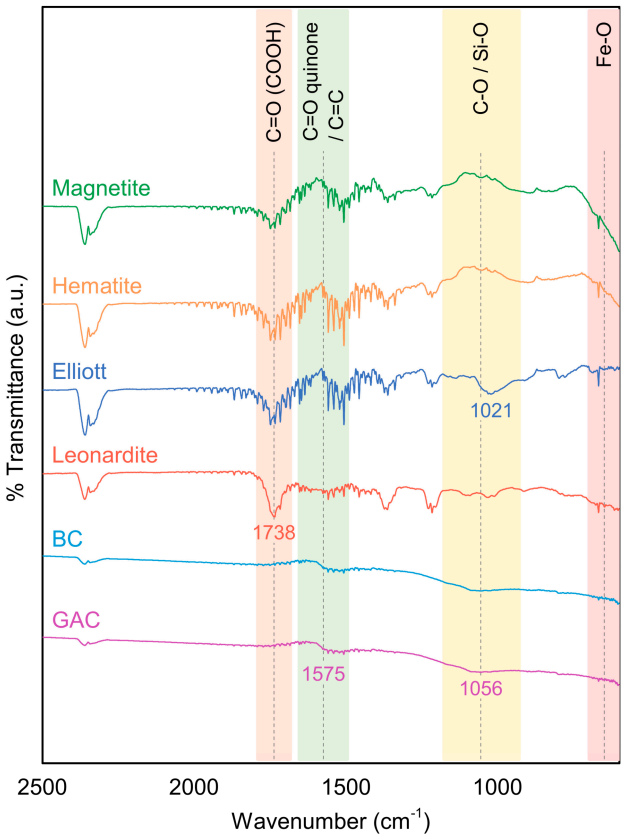


Figure 7. FTIR spectra (2500–600 cm^{-1}) of GAC, BC, Leonardite, Elliott, hematite, and magnetite. Shaded areas indicate the absorption regions of the key functional groups, and the dashed line in each area marks the characteristic band of that group discussed in the text: carboxylic C=O at 1738 cm^{-1} (Leonardite), quinone C=O/aromatic C=C at 1575 cm^{-1} (GAC), C–O at 1056 cm^{-1} (GAC; the Si–O band of Elliott appears at 1021 cm^{-1}), and Fe–O below 700 cm^{-1} (hematite and magnetite; the Fe–O maxima at 540–580 cm^{-1} lie below the measured range). The doublet at ~2360 cm^{-1} corresponds to atmospheric CO_2.

Overall, the fermentative performance suggests that the relationship between ETC measured with EtOH/HAc and caproic acid production may be associated with the dominant chemical properties of each material. Considering all materials (Figure 8A), ETC alone does not directly correlate with caproic acid synthesis (Pearson, r = −0.645, $p = 0.167$, $R^2 = 0.416$), as the overall trend is distorted by materials with specific inhibitory surface chemistries, most notably the carboxyl-rich matrix of Leonardite, which suppressed caproic acid production. However, when evaluating a subset of materials that effectively stimulated chain elongation (Figure 8B), a strong, statistically significant positive linear correlation emerged (Pearson, r = 0.959, $p = 0.041$, $R^2 = 0.9197$). This trend suggests that, for materials that actively promote chain elongation, whether through carbonaceous quinone groups (GAC, BC, Elliott) or iron-mediated electron shuttling (hematite), ETC may be associated with performance. However, this correlation is based on only four treatment means and on a subset defined after observing the results, so it should be considered exploratory. Further studies with a larger number of materials spanning distinct ETC values are needed to determine whether this relationship holds. In contrast, the strong inhibition observed with Leonardite (Figure 8A) may disrupt this relationship, possibly due to its carboxyl-rich surface chemistry.

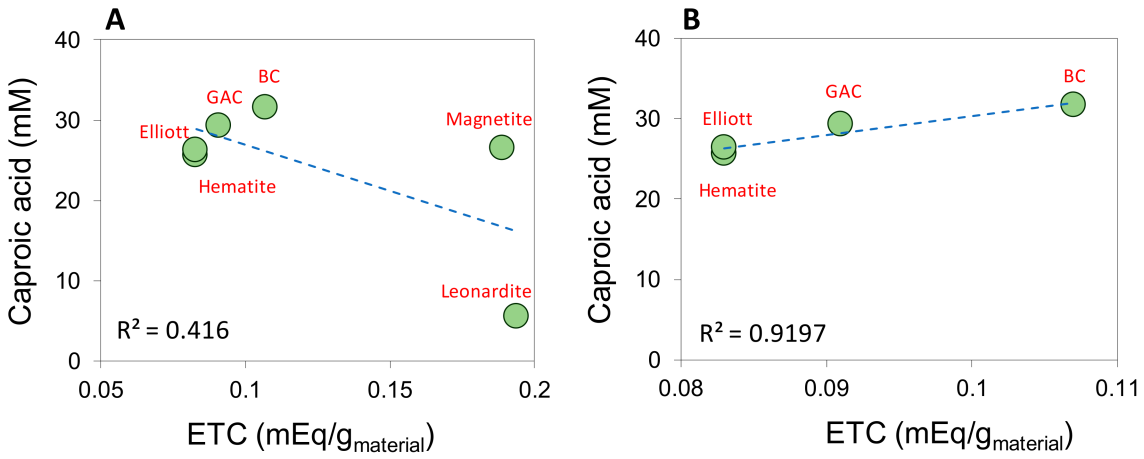


Figure 8. Relationship between the electron-transfer capacity (ETC) of the redox-active materials, measured with EtOH/HAc, and the maximum caproic acid concentration. (**A**) Global dataset including all six evaluated materials. (**B**) Subset of materials that stimulated chain elongation. Each point represents the treatment mean.

Studies using biochar, GAC, and pyrochar reported material concentrations of 15–30 g/L [7], compared with 5 g/L of GAC in this study. Carbon-based materials may support microbial communities through their high surface area and porosity, and the relative abundance of caproate-producing *Clostridium* and *Proteobacteria* has been reported to increase in such cultures [33,41]. The GAC used here has a surface area of 480 m^2/g and a pore volume of 0.29 cm^3/g [42]. Enrichment of acid-producing bacteria on carbon-based materials may also increase the enzymes and functional genes that stimulate reverse β-oxidation and fatty acid biosynthesis [19,33]. Oxygenated groups and porosity may further explain organic acid adsorption through acid–base interactions [43] (BC retained 21.8% of the caproic acid; Table 1), which, together with metabolism, may promote caproic acid production in GAC- and BC-amended cultures.

4. Conclusions

Redox-active materials boosted caproic acid production in ruminal sediment cultures, with carbon-based materials showing the highest performance. BC and GAC increased production by 67% and 55%, respectively, and FTIR showed quinone-type C=O groups in both, as in Elliott. Iron oxides and Elliott produced moderate gains (~37%) at just 250 mg/L, while Leonardite, rich in carboxyl groups and with only a weak quinone band, inhibited production. In the second assay, BC reached ~70 mM (94.4% above the control), but glucose, although it may supply electrons to the materials, reduced caproic acid production by 21.6–44.4%.

ETC did not predict caproic acid production across all materials, likely because of differences in surface chemistry. However, it showed a positive correlation for quinone-bearing materials and hematite. Further systematic studies using a broader library of redox materials, detailed surface characterization, and metagenomic analysis are needed to determine whether ETC can serve as a predictive metric or whether material-specific properties ultimately dominate the process. Future work should also examine continuous reactors, real wastes, and shifts in microbial communities.

Supplementary Materials: The following supporting information can be downloaded at: https://www.mdpi.com/article/10.3390/applmicrobiol6120144/s1, Figure S1: Production of propionic and valeric acids in the cultures inoculated with ruminal sediment and provided with redox-active materials; Figure S2: Initial and final pH values during caproic acid production in the cultures inoculated

with ruminal sediment and provided with redox-active materials; Figure S3: Composition of biogas during caproic acid production provided with redox-active materials. No methane was detected.

Author Contributions: Methodology and Investigation: C.N.-G., L.T.-M., I.C.-M., M.A.A.; Writing—original draft: V.A.B.-C.; D.S.-P., E.R.M.-E., R.B.G.-R.; Data curation and Formal analysis: L.H.A., M.A.A.; Conceptualization: L.H.A., V.A.B.-C.; Supervision, Writing and editing, and Project administration: L.H.A. All authors have read and agreed to the published version of the manuscript.

Funding: This research was funded by Secretaría de Ciencia, Humanidades, Tecnología e Innovación (SECIHTI, México). L.H.A. acknowledges research funding from SECIHTI (Grant No. CBF-2025-I-3627) and from Instituto Tecnológico de Sonora (PROFAPI-ITSON). V.A.B.-C. and M.A.A. acknowledge support from the postdoctoral fellowship from SECIHTI.

Institutional Review Board Statement: Not applicable.

Informed Consent Statement: Not applicable.

Data Availability Statement: The original contributions presented in this study are included in the article/Supplementary Material. Further inquiries can be directed to the corresponding authors.

Conflicts of Interest: The authors declare no conflicts of interest.

References

1. Srivastav, A.L.; Bagherian, A.; Ghosh, D. The circular bioeconomy: Pathways to sustainability and resource optimization. *Clean Technol. Environ. Policy* **2024**, *27*, 815–832. [CrossRef]
2. Makepa, D.C.; Chihobo, C.H. Barriers to commercial deployment of biorefineries: A multi-faceted review of obstacles across the innovation chain. *Heliyon* **2024**, *10*, e32649. [CrossRef] [PubMed]
3. Wang, Y.; He, Y.; Zheng, K.; Wei, W.; Ngo, H.H.; Guo, W.; Ni, B.J.; Zhu, T.; Horn, H.; Liu, Y. Ferric oxide stimulates medium-chain carboxylic acids synthesis from waste activated sludge via ethanol-driven chain elongation: Mechanisms and implications. *J. Clean. Prod.* **2023**, *389*, 136044. [CrossRef]
4. Angenent, L.T.; Richter, H.; Buckel, W.; Spirito, C.M.; Steinbusch, K.J.J.; Plugge, C.M.; Strik, D.P.B.T.B.; Grootscholten, T.I.M.; Buisman, C.J.N.; Hamelers, H.V.M. Chain Elongation with Reactor Microbiomes: Open-Culture Biotechnology to Produce Biochemicals. *Environ. Sci. Technol.* **2016**, *50*, 2796–2810. [CrossRef] [PubMed]
5. Douglas, E.J.A.; Palk, N.; Rudolph, E.R.; Laabei, M. Anti-staphylococcal fatty acids: Mode of action, bacterial resistance and implications for therapeutic application. *Microbiology* **2025**, *171*, 001563. [CrossRef] [PubMed]
6. Huang, T.H.; Wang, P.W.; Yang, S.C.; Chou, W.L.; Fang, J.Y. Cosmetic and Therapeutic Applications of Fish Oil's Fatty Acids on the Skin. *Mar. Drugs* **2018**, *16*, 256. [CrossRef] [PubMed]
7. Chang, B.R.; Deng, L.; Wu, Q.L.; Guo, W.Q.; Xue, H.Y. A review: Carbon-based materials as effective additives in anaerobic fermentation, focusing on microbial chain elongation and medium chain fatty acids production. *Chin. Chem. Lett.* **2025**, *36*, 110411. [CrossRef]
8. Nzeteu Corline Coelho, F.; Trego, A.C.; Abram, F.; Ramiro-Garcia, J.; Paulo, L.; O'Flaherty, V. Development of an enhanced chain elongation process for caproic acid production from waste-derived lactic acid and butyric acid. *J. Clean. Prod.* **2022**, *338*, 130655. [CrossRef]
9. Candry, P.; Ganigué, R. Chain elongators, friends, and foes. *Curr. Opin. Biotechnol.* **2021**, *67*, 99–110. [CrossRef] [PubMed]
10. Harahap, B.M.; Ahring, B.K. Chain elongation for production of medium chain carboxylic acids from green waste: Process and economic impacts of substrate composition, sterilization, and pH. *Biochem. Eng. J.* **2026**, *226*, 109994. [CrossRef]
11. Baleeiro, F.C.F.; Kleinsteuber, S.; Neumann, A.; Sträuber, H. Syngas-aided anaerobic fermentation for medium-chain carboxylate and alcohol production: The case for microbial communities. *Appl. Microbiol. Biotechnol.* **2019**, *103*, 8689–8709. [CrossRef] [PubMed]
12. Baleeiro, F.C.F.; Kleinsteuber, S.; Sträuber, H. Hydrogen as a Co-electron Donor for Chain Elongation with Complex Communities. *Front. Bioeng. Biotechnol.* **2021**, *9*, 650631. [CrossRef] [PubMed]
13. Ye, S.S.; Meng, Y.F.; Zhang, Y.Y.; Choi, W.; Wu, Q.L.; Ren, W.T.; Wang, H.Z.; Guo, W.Q. Conductive Materials in Microbial Chain Elongation for Medium-Chain Fatty Acids Biosynthesis: A Critical Review of Mechanisms and Metabolic Regulation. *ACS ES&T Eng.* **2026**, *6*, 2334–2351. [CrossRef]
14. Guo, T.; Liu, Y.; Yu, J.; Li, X.; Chen, Y.; Gao, M. A Review of Microbial Interactions and Enhancement Strategies for Medium-Chain Fatty Acids Production from Organic Wastes. *ACS ES&T Eng.* **2026**, *6*, 2352–2370. [CrossRef]
15. Burboa, V.; Alvarez, L. Methane production from antibiotic bearing swine wastewater using carbon-based materials as electrons conduits during anaerobic digestion. *Int. J. Energy Res.* **2020**, *44*, 10996–11005. [CrossRef]

16. Burboa-Charis, V.A.; Maytorena, V.M.; Armenta, M.A.; Pérez–Enciso, R.A.; Flores-Sánchez, L.A.; García-Reyes, R.B.; Cervantes, F.J.; Rittmann, B.E.; Alvarez, L.H. Impact of biochar from coconut shell and different temperatures of solar pyrolysis during the anaerobic digestion of swine wastewater. *Biomass Convers. Biorefin.* **2026**, *16*, 10. [CrossRef]
17. Lovley, D.R. Microbial Fe(III) reduction in subsurface environments. *FEMS Microbiol. Rev.* **1997**, *20*, 305–313. [CrossRef]
18. Hernández-Montoya, V.; Alvarez, L.H.; Montes-Morán, M.A.; Cervantes, F.J. Reduction of quinone and non-quinone redox functional groups in different humic acid samples by Geobacter sulfurreducens. *Geoderma* **2012**, *183–184*, 25–31. [CrossRef]
19. Wu, S.L.; Wei, W.; Xu, Q.; Huang, X.; Sun, J.; Dai, X.; Ni, B.J. Revealing the Mechanism of Biochar Enhancing the Production of Medium Chain Fatty Acids from Waste Activated Sludge Alkaline Fermentation Liquor. *ACS ES&T Water* **2021**, *1*, 1014–1024. [CrossRef]
20. Franza, T.; Gaudu, P. Quinones: More than electron shuttles. *Res. Microbiol.* **2022**, *173*, 103953. [CrossRef] [PubMed]
21. Koch, C.; Kuchenbuch, A.; Kracke, F.; Bernhardt, P.V.; Krömer, J.; Harnisch, F. Predicting and experimental evaluating bio-electrochemical synthesis—A case study with *Clostridium kluyveri*. *Bioelectrochemistry* **2017**, *118*, 114–122. [CrossRef] [PubMed]
22. Jin, X.; Yin, X.; Ling, L.; Mao, H.; Dong, X.; Chang, X.; Chen, M.; Fang, S. Adding glucose delays the conversion of ethanol and acetic acid to caproic acid in Lacrimispora celerecrescens JSJ-1. *Appl. Microbiol. Biotechnol.* **2023**, *107*, 1453–1463. [CrossRef] [PubMed]
23. Lovley, D.R.; Coates, J.D.; Blunt-Harris, E.L.; Phillips, E.J.P.; Woodward, J.C. Humic substances as electron acceptors for microbial respiration. *Nature* **1996**, *382*, 445–448. [CrossRef]
24. Klüpfel, L.; Keiluweit, M.; Kleber, M.; Sander, M. Redox properties of plant biomass-derived black carbon (biochar). *Environ. Sci. Technol.* **2014**, *48*, 5601–5611. [CrossRef] [PubMed]
25. Schröder, I.; Johnson, E.; de Vries, S. Microbial ferric iron reductases. *FEMS Microbiol. Rev.* **2003**, *27*, 427–447. [CrossRef] [PubMed]
26. Yang, P.; Leng, L.; Tan, G.Y.A.; Dong, C.; Leu, S.Y.; Chen, W.H.; Lee, P.H. Upgrading lignocellulosic ethanol for caproate production via chain elongation fermentation. *Int. Biodeterior. Biodegrad.* **2018**, *135*, 103–109. [CrossRef]
27. San-Valero, P.; Fernández-Naveira, Á.; Veiga, M.C.; Kennes, C. Influence of electron acceptors on hexanoic acid production by *Clostridium kluyveri*. *J. Environ. Manag.* **2019**, *242*, 515–521. [CrossRef] [PubMed]
28. Ma, H.; Lin, Y.; Jin, Y.; Gao, M.; Li, H.; Wang, Q.; Ge, S.; Cai, L.; Huang, Z.; Van Le, Q.; et al. Effect of ultrasonic pretreatment on chain elongation of saccharified residue from food waste by anaerobic fermentation. *Environ. Pollut.* **2021**, *268*, 115936. [CrossRef] [PubMed]
29. Da Silva, A.H.; Miranda, E.A. Adsorption/Desorption of Organic Acids onto Different Adsorbents for Their Recovery from Fermentation Broths. *J. Chem. Eng. Data* **2013**, *58*, 1454–1463. [CrossRef]
30. Andrews, G.F.; Elkcechen, S. Solid Adsorbents in Batch Fermentations. *Chem. Eng. Commun.* **1984**, *29*, 139–151. [CrossRef]
31. Li, M.; Li, T.; Zheng, J.; Qiao, Z.; Zhang, K.; Luo, H.; Zou, W. Genome Analysis and Optimization of Caproic Acid Production of *Clostridium butyricum* GD1-1 Isolated from the Pit Mud of Nongxiangxing Baijiu. *J. Microbiol. Biotechnol.* **2023**, *33*, 1337–1350. [CrossRef] [PubMed]
32. Yuan, S.; Jin, Z.; Ali, A.; Wang, C.; Liu, J. Caproic Acid-Producing Bacteria in Chinese Baijiu Brewing. *Front. Microbiol.* **2022**, *13*, 883142. [CrossRef] [PubMed]
33. Meng, F.; Wang, L.; Xu, J.; Li, X.; Hao, J. Enhanced electron transfer mediated by surface functional groups of targetedly modified sludge-based biochar for sustainable microbial chain elongation. *Bioresour. Technol.* **2026**, *441*, 133600. [CrossRef] [PubMed]
34. Yu, L.; Yuan, Y.; Tang, J.; Wang, Y.; Zhou, S. Biochar as an electron shuttle for reductive dechlorination of pentachlorophenol by Geobacter sulfurreducens. *Sci. Rep.* **2015**, *5*, 16221. [CrossRef] [PubMed]
35. Ali, R.; Aslam, Z.; Shawabkeh, R.A.; Asghar, A.; Hussein, I.A. BET, FTIR, and RAMAN characterizations of activated carbon from waste oil fly ash. *Turk. J. Chem.* **2020**, *44*, 279–295. [CrossRef] [PubMed]
36. Aeschbacher, M.; Graf, C.; Schwarzenbach, R.P.; Sander, M. Antioxidant Properties of Humic Substances. *Environ. Sci. Technol.* **2012**, *46*, 4916–4925. [CrossRef] [PubMed]
37. Azman, S.; Khadem, A.F.; Plugge, C.M.; Stams, A.J.M.; Bec, S.; Zeeman, G. Effect of humic acid on anaerobic digestion of cellulose and xylan in completely stirred tank reactors: Inhibitory effect, mitigation of the inhibition and the dynamics of the microbial communities. *Appl. Microbiol. Biotechnol.* **2016**, *101*, 889–901. [CrossRef] [PubMed]
38. Kalska-Szostko, B.; Wykowska, U.; Satula, D.; Nordblad, P. Thermal treatment of magnetite nanoparticles. *Beilstein J. Nanotechnol.* **2015**, *6*, 1385–1396. [CrossRef] [PubMed]
39. Weber, K.A.; Achenbach, L.A.; Coates, J.D. Microorganisms pumping iron: Anaerobic microbial iron oxidation and reduction. *Nat. Rev. Microbiol.* **2006**, *4*, 752–764. [CrossRef] [PubMed]
40. Cheng, S.; Bai, S.; Xu, X.; Gu, X.; Duan, X.; Duan, H.; Li, X.; Xue, G.; Fernández-Morales, F.J.; Makinia, J. Ferric oxide enhances mixed fungal-bacterial microbiome for medium-chain fatty acid production via endogenous electron donors. *Chem. Eng. J.* **2026**, *533*, 174681. [CrossRef]

41. Wu, Q.; Feng, X.; Chen, Y.; Liu, M.; Bao, X. Continuous medium chain carboxylic acids production from excess sludge by granular chain-elongation process. *J. Hazard. Mater.* **2021**, *402*, 123471. [CrossRef] [PubMed]
42. Orrantia, M.; Armenta, M.A.; Alvarez, L.H.; Burboa-Charis, V.A.; Meza-Escalante, E.R.; Olivas, A.; Arroyo, E.; Maytorena, V.M. Enhanced methane production via anaerobic digestion assisted with Fe3O4 nanoparticles supported on microporous granular activated carbon. *Fuel* **2024**, *360*, 130517. [CrossRef]
43. López-Velandia, C.; Moreno-Barbosa, J.; Sierra-Ramirez, R.; Giraldo, L.; Moreno-Piraján, J.C. Adsorption of volatile carboxylic acids on activated carbon synthesized from watermelon shells. *Adsorpt. Sci. Technol.* **2014**, *32*, 227–242. [CrossRef]

Disclaimer/Publisher's Note: The statements, opinions and data contained in all publications are solely those of the individual author(s) and contributor(s) and not of MDPI and/or the editor(s). MDPI and/or the editor(s) disclaim responsibility for any injury to people or property resulting from any ideas, methods, instructions or products referred to in the content.